Multi-physics modelling and experimental validation of electrovibration based haptic devices

Teja Vodlak, Zlatko Vidrih, Eric Vezzoli, Betty Lemaire-Semail, Djordje Peric

PII: S2352-5738(16)30041-5
DOI: doi:10.1016/j.biotri.2016.09.001
Reference: BIOTRI 37

To appear in: *Biotribology*

Received date: 14 May 2016
Revised date: 21 September 2016
Accepted date: 26 September 2016

Please cite this article as: Vodlak, Teja, Vidrih, Zlatko, Vezzoli, Eric, Lemaire-Semail, Betty, Peric, Djordje, Multi-physics modelling and experimental validation of electrovibration based haptic devices, *Biotribology* (2016), doi:10.1016/j.biotri.2016.09.001

Multi-physics modelling and experimental validation of electrovibration based haptic devices

Teja Vodlak[a,*], Zlatko Vidrih[a], Eric Vezzoli[b], Betty Lemaire-Semail[b], Djordje Peric[a]

[a] *Swansea University, College of Engineering, Singleton Park, Swansea SA2 8PP, UK*
[b] *L2EP-IRCICA, Université Lille 1, 59650 Villeneuve d'Ascq, France*

Abstract

Electrovibration tactile displays exploit the polarisation of the finger pad, caused by an insulated high voltage supplied plate. This results in electrostatic attraction, which can be used to modulate the users perception of an essentially flat surface and induce texture sensation. Two analytical models of electrovibration, based on parallel plate capacitor assumption, are demonstrably taken and assessed by comparisons with experimental results published in literature. In addition, an experimental setup was developed to measure the electrostatic force between the finger pad and a high voltage supplied plate in a static and out-of-contact state in order to support the use of parallel plate capacitor model. Development, validation, and application of a computational framework for modelling tactile scenarios on real and virtual surfaces rendered by electrovibration technique is presented. The framework incorporates fully parametric model in terms of materials and geometry of the finger pad, virtual and real surfaces, and can serve as a tool for virtual prototyping and haptic rendering in electrovibration tactile displays. This is achieved by controlling the applied voltage signal in order to guarantee similar lateral force cues in real and simulated surfaces.

Keywords: multi-physics modelling, electrovibration, friction, haptic rendering
2010 MSC: 00-01, 99-00

1. Introduction

When exploring the shape of an object, we perceive geometrical and force cues. Although these cues are correlated, it had been long assumed that the shape perception relies on geometrical features only. Robles-De-La-Torre and Hayward [1] refuted this assumption by showing, that regardless of the surface geometry, only force and force-related information were enough to determine shape perception through active touch. Later, Wiertlewski and Hayward [2] found that it

*Corresponding author
Email addresses: t.vodlak@swansea.ac.uk (Teja Vodlak), z.vidrih@swansea.ac.uk (Zlatko Vidrih), eric.vezzoli@etudiant.univ-lille1.fr (Eric Vezzoli), betty.semail@polytech-lille.fr (Betty Lemaire-Semail), d.peric@swansea.ac.uk (Djordje Peric)

is possible to characterise the tactual properties of the textures by profiling the tangential force between the exploring finger and the surface. For texture recognition, it suffices to provide spatial information only as it can be used for perceptual purposes due to the mechanical properties of the finger.

Following the idea of Wiertlewski et al. [3] of encoding the texture in terms of lateral force, technologies for haptic feedback, based on the modulation of friction between the finger pad and tactile display, have been developed. Two most promising techniques are: (i) ultrasonic vibration [4–6] and (ii) electrovibration [7–17]. Although the governing mechanisms for both techniques are different as the former reduces while the latter increases the perceived friction, it has been proven that the perception is similar for both techniques and related to friction change only [18]. In this work the attention is given to electrovibration only. Physical implementation of electrovibration does not include any moving parts and mechanical actuators, has very low power consumption, and the scale-up of the process is feasible. Hence, it may be considered as a valid approach when aiming to provide the user with high fidelity haptic feedback in next generation mass market devices.

Although the phenomenon of electrical attraction between the skin and a charged surface was first reported almost hundred years ago by Johnsen and Rahbek [19] and later theoretically and phenomenologically explained by Mallinckrodt et al. [20] in mid-fifties, it has received only limited attention in computer user interface industry until the recent progress in tactile display development and optimisation in finger position tracking. First reported attempt to exploit the phenomenon in tactile displays for visually impaired was performed by Strong and Troxel [16]. The psychophysical threshold experiments showed that the intensity of texture sensation is strongly correlated with the peak applied voltage signal, as well as with its frequency, and the electrode area. The phenomenon was also investigated by Grimnes [21], who introduced the term *electrovibration*. Grimnes was mainly investigating the effect on non-palmar sites of hand (knuckles) as he concluded that due to the large thickness of *stratum corneum* on palmar side the response was poor and irregular. In a preliminary report Beebe et al. [9] proposed a haptic tactile display based on the idea of Strong and Troxel [16], but did not present any concrete experimental measurements. Tang and Beebe [22] continued the research by optimising the display and performing psychophysical evaluations of the thresholds, line separation, and pattern recognition in similar manner as Strong and Troxel [16], to allow for comparison. In current applications, all screen area is equally charged, allowing only single-finger stimulation, although the initial attempts allowed for a local fingertip stimulation with matrix of electrodes [7, 10, 16, 22].

Despite numerous possible applications of haptic displays, little has been done in designing and evaluating algorithms for generating high fidelity tactile sensations. Romano and Kuchenbecker [23] introduced haptography, a technique that incorporates record-and-replay procedure, in which

recorded values of quantities such as forces, displacements, accelerations, measured during real surface exploration are replayed during exploration of a virtual surface. Kim et al. [11] proposed an algorithm for rendering 3D ridges as a function of surface gradient profile and a friction model, based on psychophysical experiments. Another widely used technique uses the greyscale of the displayed image and evaluates the applied voltage (friction) at a screen location in dependence to the gray levels of the pixels.

Yet, the mathematical modelling of electrovibrations still represents an open problem. Mallinckrodt et al. [20] observed that individuals do not perceive the stimulus in the same way and that simulation on different parts of hand, or even body, yields different response. Doubling of the frequency was also reported, as well as the absence of the phenomenon when finger is stationary or wet. This led them to conclude that the resin-like sensation perceived when exploring a charged surface is not a consequence of electrostimulation of mechano-receptors, but rather of friction increase due to the electrostatic force. They argued that the electrostatic force acts in a parallel plate capacitor (Fig. 1a), between two conductive plates (charged metal plate and the conducting tissue of the body) and one or two dielectrics (insulating layer on the metal surface and *stratum corneum*), which is widely accepted by the research community nowadays.

Analytical models based on parallel plate capacitor theory assumption have been proposed for modelling of electrovibrations, but the research community is still ambivalent which approach best describes the phenomenon (§2.1). For this reason, two models were demonstrably taken and assessed against experimental results reported by Strong and Troxel [16], Meyer et al. [13] and current study. Considering the phenomenological nature of the proposed models and its parameters being open to interpretation, e.g. contact area, electrical and material skin properties, effective voltage of the system, the experimental results are used to assess the physical meaning of the parameters in analytical modelling by inverse analysis (§3.2).

Little has been reported on measuring the electrostatic force between the finger pad and voltage supplied plate. Lack of experimental data is mostly due to the fact that the force is hard to measure since it is inner to the system, and that measuring it requires very high precision sensors. Moreover, there is a topical question regarding tribological properties of the finger [24, 25] and unpredictability of skin properties among population. Meyer [26] considered different procedures to measure the force, and finally decided on indirect assessment of electrostatic force by measuring its effect on friction. Reported tribological experimental measurements confirm the quadratic relationship between the imposed force and the applied voltage, and also demonstrate a large person to person variability. Shultz et al. [27] have also performed tribological measurements, although the range of forces used in their experiment are much larger than the forces anticipated in touchscreen exploration. It should be noted, that [27] considers the electroadhesion based haptic

displays, which differ from Coulomb force based displays, that are the topic of current paper.

One of the questionable assumptions in modelling electrovibration is the use of an infinite parallel plate capacitor model to describe the problem which is neither parallel nor infinite, as finger pad is curved and has fingerprints. In order to evaluate the assumption an experimental setup was designed (§2.2) with a twofold goal, namely (i) to estimate the fringing effects due to finger pad curvature, and (ii) to evaluate the influence of air, as an additional dielectric between the *stratum corneum* and the screen insulator, on the imposed electrostatic force (Fig. 1b). The experimental results are presented in section §3.1.

Due to inadequacy of global analytical parallel plate capacitor model to predict an out of contact case (§3.2.3) a discrete model is proposed based on integration of the electrostatic pressure over the finger pad area (§2.3.1), which takes into account finger pad geometry and can be relatively easily implemented in general finite element (FE) software. The discrete model adequately estimates the imposed electrostatic force when finger is in contact with the surface and when it is hovering above, the latter being an extreme non parallel case (§3.2.4).

Previous finite element studies of human touch [28–38] mostly consider two or three dimensional simulations of finger tactile exploration, studying mechanical behaviour at the point of contact or within the soft tissue. Abdolvahab [39] proposed a biomechanical model of a finger for simulation of the squeeze film effect, i.e. friction reduction due to the ultrasonic vibrations, by simulating a finger sliding over a surface with a step down, and a flat surface with a small region of decreased coefficient of friction.

Here, based on the discretised electrostatic model, a 2D multi-physics finite element framework for virtual prototyping of electrovibration friction-based haptic displays is proposed (§2.3). An algorithm for rendering haptic sensations is introduced, where friction profiles, obtained from finite element simulations of tactile scenarios, are used as an input to control the voltage signal electrovibration displays (§2.3.4). Currently proposed multi-physics computational framework is capable of simulating arbitrary tactile scenarii, including friction modulation due to electrostatic attraction directly from applied voltage signal, without changing the material properties of the surface. Haptic rendering of a flat surface with a sharp transition in friction, and a surface with fine asperities mimicking a real texture, is demonstrated in §3.2.5.

2. Methods

2.1. Analytical models of electrovibrations

By assuming a classical Coulomb friction law, the electrostatic force F_e contributes to the total lateral force F_t as

$$F_t = \mu(F_n + F_e), \tag{1}$$

where F_n denotes the applied normal force and μ the coefficient of friction. The Coulomb electrostatic force F_e between the plates of a parallel plate capacitor with a single dielectric is expressed as

$$F_e = \frac{\epsilon_0\, \epsilon\, A\, U^2}{2d^2}, \tag{2}$$

where U denotes the potential difference between the plates, i.e. the voltage applied, A plate surface area, ϵ_0 permittivity of vacuum, and ϵ and d relative permittivity and thickness of the dielectric, respectively.

Strong and Troxel [16] proposed the first mathematical model for electrostatic attraction between the finger pad and the charged surface based on the experimental results as:

$$F_e^{\mathrm{ST}} = \frac{\epsilon_0\, A\, U^2}{2\left(\frac{d^{\,\mathrm{sc}}}{\epsilon^{\,\mathrm{sc}}} + \frac{d^{\,\mathrm{i}}}{\epsilon^{\,\mathrm{i}}}\right)^2}, \tag{3}$$

taking into account both the surface insulator 'i' and the *stratum corneum* 'sc' as dielectrics.

Kaczmarek et al. [10], who were investigating the effect of voltage polarity in electrovibration tactile displays, questioned (3) by claiming that, when either $d^{\,\mathrm{sc}}$ or $d^{\,\mathrm{i}}$ approaches zero, or when $\epsilon^{\,\mathrm{sc}} = \epsilon^{\,\mathrm{i}} = \epsilon$, the expression should equal (2), but instead it differs by the factor of ϵ, i.e.

$$F_e^{\mathrm{ST}} = \frac{\epsilon_0\, \epsilon^2\, A\, U^2}{2d^2}. \tag{4}$$

The expression they proposed instead was derived from first principles by differentiating capacitor co-energy with respect to total thickness of capacitor $d = d^{\,\mathrm{i}} + d^{\,\mathrm{sc}}$, i.e. assuming distensible insulators and constant voltage:

$$F_e^{\mathrm{K}} = \frac{\epsilon_0 A U^2}{2\left(\frac{d^{\,\mathrm{sc}}}{\epsilon^{\,\mathrm{sc}}} + \frac{d^{\,\mathrm{i}}}{\epsilon^{\,\mathrm{i}}}\right)\left(d^{\,\mathrm{sc}} + d^{\,\mathrm{i}}\right)}. \tag{5}$$

Expression (5) was adopted by Bau et al. [8], Radivojevic et al. [15], Giraud et al. [40], Vezzoli et al. [17, 18] and Kim et al. [12], but questioned by Meyer et al. [13], who adopted (3) as described in [26]. Shultz et al. [27] proposed alternative derivation of the expression based on Johnsen-Rahbek effect by the means of assumed system impedance, which yields sightly modified Strong and Troxel's equation as:

$$\bar{F}_e^{\mathrm{ST}} = \frac{\epsilon_0\, A\, U^2}{2\epsilon^{\,\mathrm{a}}\left(\frac{d^{\,\mathrm{sc}}}{\epsilon^{\,\mathrm{sc}}} + \frac{d^{\,\mathrm{a}}}{\epsilon^{\,\mathrm{a}}} + \frac{d^{\,\mathrm{i}}}{\epsilon^{\,\mathrm{i}}}\right)^2}, \tag{6}$$

and introduced the air layer (denoted by 'a' in the expression (6)), as it has been reported previously, that electrostatic attraction is present even if finger pad and the charged plate are out of imminent contact [17].

Air layer can also be included in case of (5), where, again based on derivation from the first principles, the equation reads

$$\bar{F}_e^{\,\mathrm{K}} = \frac{\epsilon_0\, A\, U^2}{2\left(\frac{d^{\,\mathrm{sc}}}{\epsilon^{\,\mathrm{sc}}} + \frac{d^{\,\mathrm{a}}}{\epsilon^{\,\mathrm{a}}} + \frac{d^{\,\mathrm{i}}}{\epsilon^{\,\mathrm{i}}}\right)\left(d^{\,\mathrm{sc}} + d^{\,\mathrm{a}} + d^{\,\mathrm{i}}\right)}. \tag{7}$$

Although the assumption of distensible dielectrics in the case of (5) might be acceptable, one might doubt it in case of (7): the insulator and the *stratum corneum* are solid dielectrics, while their electrical properties might be altered by mechanical stress, and displacement would mostly happen in the air gap (liquid dielectric). The appropriate equation should therefore be derived by differentiation of the co-energy with respect to the air gap only, which results in (6), unless the space filled with liquid dielectric is assumed [26, 41].

Similar discussion and disputes about the choice of appropriate model also appear in other fields, such as electrostatic chuck applications [42], where it is argued that both formulations have their validity, depending on their use, for example in FE simulations.

2.2. Electrostatic force in out-of-contact state

The experimental setup was designed to measure electrostatic attraction, induced by a high voltage, supplied between a finger pad and a plate. Due to the nature of the electrostatic force and tribological finger pad properties, the force is hard to measure once the bodies are brought into contact. Hence, static out-of-contact approach is considered, i. e. the finger and the plate are both motionless and do not form immediate contact.

Description. The main components of the setup, as depicted in Fig. 2 comprise a chemical scale (BP410, Sartorius, Germany) acting as a force sensor, a tactile plate attached to the scale, a vertical bench placed over the scale and equipped with two micro-positioners (M-SDS40, Newport, USA), and a finger-holder. The tactile plate comprises a copper tape, 10×4 cm in size, which is glued to the scale and covered with a plastic insulator ($d^{\,\mathrm{i}} = 0.090$ mm, $\epsilon^{\,\mathrm{i}} = 3.35$). The plate is connected to a high voltage amplifier (HVA2kV, Ultravolt, USA); see [40] for more details on safety issues. The finger-holder has a shape of a wedge, is clamped to the horizontal bench with magnets and positions the finger so that the angle between longitudinal axis of the finger and the plate is 30°.

Participants. Eleven volunteers were recruited for the study, including eight males and three females, aged between 22 and 57 years with a median age of 28 years. They all gave their informed consent and did not report any skin condition or tactile deficit.

Procedure. Participants were placed in front of the setup, as illustrated in Fig. 2. Oral description of the setup and explanation of one's task was given to each of them. Using digital caliper, dimensions of each participant left index finger pad were taken, namely, width and height of the finger at proximal nail bed and length of the finger between interphalangeal joint and the finger tip (Table 1). Finger pad was then wiped with alcoholic solution before attached to the finger-holder with a tape; to prevent any movements the nail was fastened using double-sided adhesive tape. We allowed a few minutes for the finger to adapt to the new conditions and the skin to regain its natural humidity. Participants were asked to position their left hand on a setup and to put their right hand on a metallic plate connected to the mass to close the circuit.

Electrostatic force measurements (Table 1) were collected and analysed in real-time using Matlab [43]. Two different applied voltages (HV = 2000 V and LV = 1414 V) and two different distances between the finger pad and the plate (HD = 0.50 mm and LD = 0.25 mm) in three combinations (HVHD, HVLD, LVLD) were considered. Each recording lasted roughly 60 s. The voltage was applied in terms of step-function with on-and-off period of 5 s.

Best estimate finger geometry. Finger pad shape was approximated with ellipsoidal geometry. Average finger geometry was estimated based on the measured finger dimensions of each participant (Table 1). Best estimate lateral and vertical axis lengths of the finger cross-section at proximal nail fold were taken to be arithmetic mean of their respective measurements, $2a = \mathrm{AM}[a_i]$ and $2b = \mathrm{AM}[b_i]$, respectively. Best estimate longitudinal axis length was taken to be horizontal projection of the arithmetic mean of longitudinal axis lengths, i.e. $2c = \mathrm{Cos}\,30^\circ \mathrm{AM}[c_i]$.

2.3. Finite element modelling of a finger pad–haptic display interaction

The computational framework proposed here incorporates coupling of mechanical (§2.3.1) and electrical domain through discretised parallel plate capacitor model assumption (§2.3.2).

The framework was developed in Mathematica using Wolfram Language [44], including post-processing, data manipulation and visualisation. Numerical analyses were performed using Mathematica finite element environment AceFEM [45], a general multi-physics and multi-field finite element system for Mathematica, and AceGen, automatic code generation package for symbolic generation of new finite elements.

Finite element formulations for modelling finger tissue and contact element without electrostatic component were obtained from AceShare system library. Procedures for parametrised 2D finger pad cross-section structured mesh generation and parametric tactile scenario input, that were developed and implemented in this work, enable the user to perform quick sensitivity and inverse modelling studies [46].

The model incorporates the following free parameters: (i) tissue layer materials, including material parameter values and different constitutive laws, (ii) geometrical properties, including size of the finger pad, thickness of tissue layers, density and depth of finger print ridges, (iii) contact properties, (iv) loading scenario, and (v) applied voltage signal.

2.3.1. Mechanical domain

A 3D multi-scale finite element framework system for simulation of tactile scenarii has been developed earlier in order to obtain spike time predictions of mechano-receptors during finger pad exploration of different surfaces [34]. Present study employs a 2D version of the framework, as due to its computational complexity, the 3D geometry can not be sufficiently detailed, namely it lacks epidermal and papillary ridges. Moreover, a 2D model is also more practical option for performing parametric studies.

The FE model of the finger pad comprises most characteristic subdomains to assure sufficient anatomical accuracy (Fig. 3). The subdomains are (i) cornified and (ii) vital layer of epidermis, i.e. stratum corneum and (vital) epidermis, respectively; (iii) dermis; (iv) hypodermis, i.e. the dermal white adipose tissue or subcutaneous tissue; (v) nail; and (vi) bone.

The material and geometrical properties used in the model were obtained from literature [32, 47], see Table 2. Since the finger pad can exhibit large elastic deformations the hyperelastic Neo-Hookean constitutive law is employed [35, 48, 49]. Built-in two dimensional quadrilateral plane strain F-bar finite elements [50] are utilised. The contact is modelled using contact finite elements with node-to-segment formulation, implemented in terms of Coulomb friction and augmented Lagrange multiplier method [51, 52].

2.3.2. Electrical domain

Integration of the electrical domain within the framework incorporates the finger pad–touch screen interaction within the weakly coupled scheme using staggered procedure.

Equations (3) and (5) or (6) and (7) assume parallel plates, which is appropriate approximation when finger pad is in contact with the screen (although it neglects the finger pad asperities), but due to its distinct curvature, the approximation is far from reality when the finger pad is hovering above the plate (Fig 1b). Denoting $\mathbf{x} = (x, y)$ as a vector of relative position on the finger pad, an expression for the vertical component of electrostatic force acting on the plates of assumed capacitor can be written as a surface integral of electrostatic pressure as

$$\bar{F}_e^{\mathrm{ST}} = \iint_A \frac{\epsilon_0 U^2 \,\mathrm{d}x\mathrm{d}y}{2\left(\frac{d^{\mathrm{sc}}(\mathbf{x})}{\epsilon^{\mathrm{sc}}} + \frac{d^{\mathrm{a}}(\mathbf{x})}{\epsilon^{\mathrm{a}}} + \frac{d^{\mathrm{i}}}{\epsilon^{\mathrm{i}}}\right)^2} \tag{8a}$$

or

$$\bar{F}_e^{\,\mathrm{K}} = \iint\limits_A \frac{\epsilon_0 U^2 \,\mathrm{d}x\mathrm{d}y}{2\big(\frac{d^{\,\mathrm{sc}}(\mathbf{x})}{\epsilon^{\,\mathrm{sc}}} + \frac{d^{\,\mathrm{a}}(\mathbf{x})}{\epsilon^{\,\mathrm{a}}} + \frac{d^{\,\mathrm{i}}}{\epsilon^{\,\mathrm{i}}}\big)\big(d^{\,\mathrm{sc}}(\mathbf{x}) + d^{\,\mathrm{a}}(\mathbf{x}) + d^{\,\mathrm{i}}\big)} \tag{8b}$$

depending on the adopted model. Equations (8a) and (8b) incorporate the change of the geometry of the finger pad–tactile display system under applied loading scenario. Hence, the system is assumed to behave as parallel circuit of parallel plate capacitors with varying thicknesses of dielectrics in series, i.e. *stratum corneum* thickness and air gap are functions of their position on the finger pad, $d^{\,\mathrm{sc}} = d^{\,\mathrm{sc}}(x, y)$ and $d^{\,\mathrm{a}} = d^{\,\mathrm{a}}(x, y)$ (Fig. 4).

Note that the fringing effect is neglected, and only the normal component of the electrostatic force is considered, since it is assumed horizontal components cancel out due to the symmetry of the fingerprint ridges. [1] In-plane deformations of *stratum corneum* caused by horizontal component of the electrostatic force are minimal due to its high axial stiffness. Similar can be assumed regarding the deformations of the insulator, which is here modelled as completely rigid.

In order to implement the electrostatic force into FE code (Fig. 4), (8a) and (8b), which, when applied to parallel plates, simplify to (6) and (7), respectively, need to be discretised over contact nodes j, ${}^h\bar{F}_e = \sum_j {}^h\bar{F}_{ej}$, hence

$${}^h\bar{F}_e^{\,\mathrm{ST}} = \sum_j \frac{\epsilon_0\, U^2\, A_j}{2\big(\frac{d^{\,\mathrm{sc}}{}_j}{\epsilon^{\,\mathrm{sc}}} + \frac{d^{\,\mathrm{a}}{}_j}{\epsilon^{\,\mathrm{a}}} + \frac{d^{\,\mathrm{i}}}{\epsilon^{\,\mathrm{i}}}\big)^2} \tag{9a}$$

or

$${}^h\bar{F}_e^{\,\mathrm{K}} = \sum_j \frac{\epsilon_0\, U^2\, A_j}{2\big(\frac{d^{\,\mathrm{sc}}{}_j}{\epsilon^{\,\mathrm{sc}}} + \frac{d^{\,\mathrm{a}}{}_j}{\epsilon^{\,\mathrm{a}}} + \frac{d^{\,\mathrm{i}}}{\epsilon^{\,\mathrm{i}}}\big)\big(d^{\,\mathrm{sc}}{}_j + d^{\,\mathrm{a}}{}_j + d^{\,\mathrm{i}}\big)}. \tag{9b}$$

Electrostatic force is implemented within the above-mentioned finite contact element (§2.3) as follows: under applied voltage each node forming the contact surface is additionally supplied with adjoint discrete part of electrostatic force, which is calculated using either (9a) or (9b), taking into account contributing area A_j, air gap $d^{\,\mathrm{a}}{}_j$ and relative thickness of *stratum corneum* $d^{\,\mathrm{sc}}{}_j$ (Fig. 4). Mechanical and electrical domains are coupled using staggered procedure. At each incremental step, the converged solution of the mechanical domain provides new geometric configuration for the electrical domain. The electrostatic forces are then re-calculated and passed back as new loads to the mechanical domain.

[1] The model of the finger is symmetric with respect to its vertical axis, as well as each finger print ridge. Since the applied voltage is constant along the plate, horizontal components of electrostatic force in opposite (mirrored) contact nodes are assumed to be equal and opposite.

2.3.3. Evaluation of the air layer

To evaluate influence the air layer (i.e. gaps between fingerprint ridges) as an insulator during the light touch exploration, the condition of ${}^{h}\bar{F}_{ej} = 0$ is enforced for each node j which is not in contact with the reference standard, i.e. the electrostatic force is calculated as in (3) or (5),

$$ {}^{h}F_e^{\mathrm{K}} = \sum_j \frac{\epsilon_0 \, U^2 \, A_j}{2\left(\frac{d^{\mathrm{sc}}{}_j}{\epsilon^{\mathrm{sc}}} + \frac{d^{\mathrm{i}}}{\epsilon^{\mathrm{i}}}\right)\left(d^{\mathrm{sc}}{}_j + d^{\mathrm{i}}\right)}. \tag{10} $$

It can be shown that as the normal force increases, the influence of air layer decreases since the nodes in contact contribute to total electrostatic force significantly more than those out of contact.

By assuming that the contact area between a finger pad and a flat surface may be described by a power law as a function of applied normal force $A = kF_n^m$ ([25], further discussed in §2.3.4), and postulating that it can be identified as a main contributing factor to the nominal difference between ${}^{h}\bar{F}_e$ and ${}^{h}F_e$, it is proposed that the difference between ${}^{h}\bar{F}_e$ and ${}^{h}F_e$ also follows the power law behaviour in terms of the normal force, i.e.

$$ \frac{{}^{h}\bar{F}_e - {}^{h}F_e}{{}^{h}F_e} = \alpha F_n^{-\beta}. \tag{11} $$

The influence of the air layer is numerically investigated in §3.2.5, where the coefficients α and β are determined for the cases of models with and without fingerprints.

2.3.4. Haptic rendering for an electrovibration tactile display

Preprocessing for virtual prototyping is performed by monitoring the normal force ${}^{\mathrm{rs}}F_n$ and friction ${}^{\mathrm{rs}}F_t$ when sliding the model of a finger pad over a reference standard, i.e. the surface with specific mechanical and geometrical properties. Then, assuming normal force ${}^{\mathrm{rs}}F_n$ to be constant and magnitude of perceived frictional force ${}^{\mathrm{rs}}F_t$ to be a function of finger pad position $\mathbf{r} = \mathbf{r}(t)$ with respect to the RS, the phenomenon can be treated as modulation of the friction coefficient,

$$ {}^{\mathrm{rs}}F_t(t, \mathbf{r}(t)) = {}^{\mathrm{rs}}\mu(t, \mathbf{r}(t)) {}^{\mathrm{rs}}F_n. \tag{12} $$

To render a sensation on a flat haptic display (HD) that is equivalent to the one perceived when using reference standard (RS), the frictional force ${}^{\mathrm{hd}}F_t(t, \mathbf{r}(t))$ must equal ${}^{\mathrm{rs}}F_t(t, \mathbf{r}(t))$. Hence, as ${}^{\mathrm{hd}}F_n$ and ${}^{\mathrm{hd}}\mu$ are assumed constant, friction ${}^{\mathrm{hd}}F_t(t, \mathbf{r}(t))$ is modulated by electrostatic load contribution to the normal force as a function of finger pad position $\mathbf{r}(t)$. Equation (1) therefore reads

$$ {}^{\mathrm{hd}}F_t(t, \mathbf{r}(t)) = {}^{\mathrm{hd}}\mu({}^{\mathrm{hd}}F_n + F_e(t, \mathbf{r}(t))), \tag{13} $$

reflecting location and time dependence [15]. The magnitude of the electrostatic force can be modulated by changing the applied voltage U and can be written in terms of expression (5) as[2]

$$F_e^{\mathrm{K}}(t,\mathbf{r}(t)) = \frac{\epsilon_0\, A\, U(t,\mathbf{r}(t))^2}{2\left(\frac{d^{\mathrm{sc}}}{\epsilon^{\mathrm{sc}}}+\frac{d^{\mathrm{i}}}{\epsilon^{\mathrm{i}}}\right)\left(d^{\mathrm{sc}}+d^{\mathrm{i}}\right)}. \tag{14}$$

Here, the influence of air layer is neglected for it is challenging to estimate it in advance, and the thickness of stratum corneum d^{sc} is presumed constant. Contact area A is in general unknown as it strongly depends on applied normal load F_n. As reported in Adams et al. [25], the relationship between the contact area and the normal force may be written in the form of a power law,

$$A = kF_n^m. \tag{15}$$

Taking (13), substituting $F_e(t,\mathbf{r}(t))$ with (14), and writing A in a power law form, yields the following expression

$${}^{\mathrm{hd}}F_t^{\mathrm{K}}(t,\mathbf{r}(t)) = {}^{\mathrm{hd}}\mu\left[{}^{\mathrm{hd}}F_n + \frac{\epsilon_0\, k\, [{}^{\mathrm{hd}}F_n]^m\, U(t,\mathbf{r}(t))^2}{2\left(\frac{d^{\mathrm{sc}}}{\epsilon^{\mathrm{sc}}}+\frac{d^{\mathrm{i}}}{\epsilon^{\mathrm{i}}}\right)\left(d^{\mathrm{sc}}+d^{\mathrm{i}}\right)}\right] \tag{16a}$$

or, in case we derive from (3),

$${}^{\mathrm{hd}}F_t^{\mathrm{ST}}(t,\mathbf{r}(t)) = {}^{\mathrm{hd}}\mu\left[{}^{\mathrm{hd}}F_n + \frac{\epsilon_0\, k\, [{}^{\mathrm{hd}}F_n]^m\, U(t,\mathbf{r}(t))^2}{2\left(\frac{d^{\mathrm{sc}}}{\epsilon^{\mathrm{sc}}}+\frac{d^{\mathrm{i}}}{\epsilon^{\mathrm{i}}}\right)^2}\right]. \tag{16b}$$

Considering (16a), the applied voltage $U(t,\mathbf{r}(t))$ can then be estimated as[3]

$$U^{\mathrm{K}}(t,\mathbf{r}(t)) = \sqrt{\frac{2\left(\frac{d^{\mathrm{sc}}}{\epsilon^{\mathrm{sc}}}+\frac{d^{\mathrm{i}}}{\epsilon^{\mathrm{i}}}\right)\left(d^{\mathrm{sc}}+d^{\mathrm{i}}\right)F_e^{\mathrm{K}}(r,\mathbf{r}(t))}{\epsilon_0\, k\, F_n^m}}, \tag{17}$$

where $F_n = {}^{\mathrm{hd}}F_n = {}^{\mathrm{rs}}F_n$ is postulated.

The electrostatic force $F_e(t,\mathbf{r}(t))$ needed to simulate apparent friction coefficient ${}^{\mathrm{rs}}\mu(t,\mathbf{r}(t))$ with regard to the actual friction coefficient of the screen ${}^{\mathrm{hd}}\mu$ may be calculated by equating ${}^{\mathrm{hd}}F_t(t,\mathbf{r}(t)) = {}^{\mathrm{rs}}F_t(t,\mathbf{r}(t))$. Subtracting (12) and (13) and writing the expression in terms of $F_e(t,\mathbf{r}(t))$ yields the following relationship:

$$F_e(t,\mathbf{r}(t))) = \left[\frac{{}^{\mathrm{rs}}\mu(t,\mathbf{r}(t))}{{}^{\mathrm{hd}}\mu} - 1\right]F_n. \tag{18}$$

[2]Here we show derivation for (5) only; derivation using (3) can be done in similar manner.

[3]Following the approach reported in [17] the value obtained by (19) is the effective voltage U_{eff} acting on the finger pad; for a sinusoidal voltage carrier of frequency above 10 kHz the applied voltage should be approximately $2U(t,x(t))$.

Taking into account that electrovibrations technique can only increase the apparent friction, hence the quotient between friction coefficients ${}^{\mathrm{rs}}\mu(t,\mathbf{r}(t))$ and ${}^{\mathrm{hd}}\mu$ cannot be less than 1, the voltage equation (17) can be rewritten as

$$U^{\mathrm{K}}(t,\mathbf{r}(t)) = \sqrt{\frac{2\left(\frac{d^{\mathrm{sc}}}{\epsilon^{\mathrm{sc}}}+\frac{d^{\mathrm{i}}}{\epsilon^{\mathrm{i}}}\right)\left(d^{\mathrm{sc}}+d^{\mathrm{i}}\right)\left(\frac{{}^{\mathrm{rs}}\mu(t,\mathbf{r}(t))}{{}^{\mathrm{hd}}\mu}-1\right)}{\epsilon_0\, k\, F_n^{m-1}}}. \tag{19}$$

Since the vertical loads are relatively small during tactile explorations (< 0.5 N), the linear relationship between the normal force and contact area in (15) is assumed, i.e. power law parameter $m = 1$. As the current framework incorporates 2D model under plane strain assumption, the function of finger pad position reduces to $\mathbf{r} = \mathbf{r}(t) = x(t)$. Hence, the required voltage may be calculated as follows:[4]

$$U^{\mathrm{K}}(t,\mathbf{r}(t)) = \sqrt{\frac{2\left(\frac{d^{\mathrm{sc}}}{\epsilon^{\mathrm{sc}}}+\frac{d^{\mathrm{i}}}{\epsilon^{\mathrm{i}}}\right)\left(d^{\mathrm{sc}}+d^{\mathrm{i}}\right)\left(\frac{{}^{\mathrm{rs}}\mu(t,\mathbf{r}(t))}{{}^{\mathrm{hd}}\mu}-1\right)}{\epsilon_0\, k'}} \tag{20a}$$

or, in case we derive from (3), as

$$U^{\mathrm{ST}}(t,\mathbf{r}(t)) = \sqrt{\frac{2\left(\frac{d^{\mathrm{sc}}}{\epsilon^{\mathrm{sc}}}+\frac{d^{\mathrm{i}}}{\epsilon^{\mathrm{i}}}\right)^2\left(\frac{{}^{\mathrm{rs}}\mu(t,\mathbf{r}(t))}{{}^{\mathrm{hd}}\mu}-1\right)}{\epsilon_0\, k'}} \tag{20b}$$

It may be observed, that in the case of linear relationship between contact area and normal force, the required voltage is independent of the latter.

The examples of using the framework as a tool for haptic rendering are demonstrated in §3.2.4 and §3.3.

3. Results

Here, we first report on values of electrostatic force measured in out-of-contact state using a developed setup (§2.2). This is followed by cross-comparison of analytical predictions, numerical simulations and experimental measurements of electrostatic force using two analytical models, developed computational framework and three sets of experimental data (Meyer et al. [13], Strong and Troxel [16]; current study). The section concludes with two examples of haptic rending utilising encoding as proposed in §2.3.4.

3.1. Measurements of electrostatic force in out-of contact state

The experimentally obtained measurements of electrostatic force between a finger and a high voltage supplied plate in out-of-contact state using a developed setup (§2.2) are shown in Table 1 and Fig. 5, *red* boxes.

[4] To distinguish between coefficients, k' is used for linear approximation and k for any other power law parameter m.

Average measured values were 1.81, 2.95 and 1.31 mN for considered scenarii HVHD (2000 V, 0.50 mm), HVLD (2000 V, 0.25 mm) and LVLD (1414 V, 0.25 mm), respectively. When reducing the air gap from HD (0.50 mm) to LD (0.25 mm) at HV (2000 V), the median electrostatic force increased from 1.85 ± 0.547 to 2.73 ± 1.07 mN ($\pm\sigma$). Keeping the finger at LD (0.25 mm) and reducing the voltage to LV (1414 V) lowered the median electrostatic force to 1.37 ± 0.558 mN.

3.2. Assessment of analytical models

3.2.1. Estimation of the stratum corneum thickness

Strong and Troxel [16] were able to extract the effective thickness of the *stratum corneum* $\frac{d^{\mathrm{sc}}}{\epsilon^{\mathrm{sc}}}$ from the threshold voltage using two insulators of different thicknesses, by equating the tangential forces

$$\frac{\epsilon_0 A {U_2}^2 \mu_2}{2\left(\frac{{d^{\mathrm{i}}}_2}{\epsilon^{\mathrm{i}}} + \frac{d^{\mathrm{sc}}}{\epsilon^{\mathrm{sc}}}\right)^2} = \frac{\epsilon_0 A {U_3}^2 \mu_3}{2\left(\frac{{d^{\mathrm{i}}}_3}{\epsilon^{\mathrm{i}}} + \frac{d^{\mathrm{sc}}}{\epsilon^{\mathrm{sc}}}\right)^2}. \tag{21}$$

The results of the above-mentioned experiment were reported for a single trained subject, although Strong and Troxel asserted that the other subject gave similar results in terms of forces, but different effective thickness of the *stratum corneum*. It is interesting to note that in their experiment they did not use a tribometer, but rather relied on the subjects reporting the ratio between the normal and tangential load.

Postulating $d^{\mathrm{i}} = 2{d^{\mathrm{i}}}_2 = {d^{\mathrm{i}}}_3$ and $\mu_2 = \mu_3$, expressing effective thickness from (21), and replacing parameters with reported numerical values, namely $U_2 = 73$ V, $U_3 = 110$ V, ${d^{\mathrm{i}}}_2 = 0.5$ mil and ${d^{\mathrm{i}}}_3 = 1.0$ mil, $\epsilon^{\mathrm{i}} = 4.5$, yields

$$\frac{d^{\mathrm{sc}}}{\epsilon^{\mathrm{sc}}} = \frac{d^{\mathrm{i}}}{\epsilon^{\mathrm{i}}} \cdot \frac{2\,U_2 - U_3}{U_3 - U_2} = 2.74\ \mu\mathrm{m} = 0.108\ \mathrm{mil}. \tag{22}$$

Considering $\epsilon^{\mathrm{sc}} \approx 2000$ at 200 Hz [53], it follows that the *stratum corneum* thickness should equal $d^{\mathrm{sc}} = 5.48$ mm, which is an unrealistic value, an order of magnitude larger than the one generally accepted, i.e. $\approx 300\ \mu$m in palmar regions [25, 47, 54].

On the other hand, if *stratum corneum* thickness is derived from (5), i.e.

$$\frac{\epsilon_0 A {U_2}^2 \mu_2}{2\left(\frac{{d^{\mathrm{i}}}_2}{\epsilon^{\mathrm{i}}} + \frac{d^{\mathrm{sc}}}{\epsilon^{\mathrm{sc}}}\right)\left({d^{\mathrm{i}}}_2 + d^{\mathrm{sc}}\right)} = \frac{\epsilon_0 A {U_3}^2 \mu_3}{2\left(\frac{{d^{\mathrm{i}}}_3}{\epsilon^{\mathrm{i}}} + \frac{d^{\mathrm{sc}}}{\epsilon^{\mathrm{sc}}}\right)\left({d^{\mathrm{i}}}_3 + d^{\mathrm{sc}}\right)}, \tag{23}$$

by making the same postulates and using the same numerical values as in (21), it follows that the *stratum corneum* thickness should equal 76.2 μm. This value is lower than the reported average, but plausible nonetheless.

3.2.2. Electrostatic force as friction increment

Meyer et al. [13] performed rigorous experimental parametric study which reported on the electrostatic force as a function of voltage and frequency of the input signal.

Friction. A relationship between the lateral and normal force acting on a sliding finger with and without electrovibration was presented for a single subject, indicating that the imposed electrostatic force was 0.25 N with standard error 0.01 N (Fig. 6a). Equations (3) and (5) were utilised using reported values for thickness of *stratum corneum* and insulator, i.e. $d^{\mathrm{sc}} = 0.200$ mm and $d^{\mathrm{i}} = 0.001$ mm, respectively. Contact area A was assumed to be 100 mm^2. Relative permittivities of *stratum corneum* and the insulator were varied; ϵ^{sc} was varied from 10^3 to 10^4, corresponding to the relevant frequency range and obtained from [53], while ϵ^{i} varied from 1 to 10, covering a range of values for typical insulator materials. Calculating electrostatic force using (5) gives the values that are the same order as forces measured in the above-mentioned experiment ($0.05 - 0.35$ N), whereas (3) predicts values that are up to three orders of magnitude greater ($10 - 600$ N), as depicted in Fig. 7.

Voltage dependence. Values of electrostatic force F_e in relationship to applied voltage U, experimentally obtained by [13], are juxtaposed with analytical results obtained using (3) and (5). Again, area of $A = 100$ mm^2 was assumed and *stratum corneum* thickness was varied from 0.1 to 0.5 mm in steps of 0.1 mm. Results are presented in Fig. 8, where it is established that the large person to person variability can be explained by *stratum corneum* thickness variability using (5), whereas (3) again overestimates the values by the order of magnitude. Although the effective voltage acting on the capacitor in an electrical circuit as assumed by Meyer et al. [13] is somewhat lower than the actual applied voltage, it is quite clear that (5) presents more adequate description of the phenomenon.

Contact area. An important input parameter open for interpretation is the contact area A, which is dependent on imposed normal load F_n as formulated by (15). Expressions (16b) and (16a) were fitted to experimental results taken from [13] (Fig. 6a) in order to obtain coefficient k and load index m. Obtained parameters were used to estimate the accompanying contact area, assuming $d^{\mathrm{sc}} = 0.1$ mm (taken from Fig. 8b for maximum force) and $d^{\mathrm{i}} = 0.001$ mm, whereas all other parameters were as in Table 2. Obtained coefficients are utilised in (15) and the results are juxtaposed to experimental results reported by Adams [55] in Fig. 6b. Note that (5) gives a realistic estimate of the contacting area shown in Fig. 6b by a *blue* curve, while expression (3) results in unrealistically small value for the contacting area, which is represented by an *orange* curve hardly distinguishable from the horizontal axis.

3.2.3. Electrostatic force in out-of-contact state

As discussed in §2.3.2, the closed form equations for electrostatic force (6) and (7) cannot be directly used, as it is hard to estimate the contributing area A *a priori* due to the finger pad

curvature. Two options were considered:

(i) assuming flat *stratum corneum* positioned above the plate at the distance ${d^{\mathrm{a}}}_0$, with varying surface A from 10 to 50 mm^2 in step of 10 mm^2,

(ii) assuming ellipsoidal geometry of the finger pad and varying the distance in dependence of relative position (x, y),

$$d^{\mathrm{a}}(x,y) = {d^{\mathrm{a}}}_0 + 2b - \frac{b}{a}\sqrt{a^2 - x^2} - \frac{b}{c}\sqrt{c^2 - y^2}, \tag{24}$$

with semi-axes $2a = 16.70$, $2b = 12.80$ and $2c = 22.5$ mm, based on the best estimate finger geometry (2.2).

In both cases, the voltage U and the initial distance ${d^{\mathrm{a}}}_0$ were varied, respectively, from 1000 to 2500 V (Fig. 9a) and from 0 to 0.75 mm (Fig. 9b).

Option (i) provides a good estimate of trends when changing voltage U, but fails to capture the influence in change of the distance d^{a}. Relatively low contributing area has to be used to come into the range of measured forces ($A \approx 10 - 20$ mm^2). In case of option (ii), both equations correctly predict the trend of approximately doubling of the electrostatic force when increasing the voltage from LVLD to HVLD, although (8a) overestimates the experimental values (experiment – 1.37 to 2.73, (8a) – 2.62 to 5.24 and (8b) – 1.47 to 2.95 mN), but differ in predicting the trend when reducing the air gap from HVHD to HVLD (experiment – 1.85, (8a) – 2.54 and (8b) – 1.76 mN).

In general, one can conclude that (8b) better predicts the behaviour when voltage and distance are varied (Fig. 10). The same figure also plots values for varying thickness of *stratum corneum*, $d^{\mathrm{sc}} = 0.38 \pm 0.11$ mm. Note that (8a) is unaffected by the change of the d^{sc}.

Moreover, (8b) and (8a) were used to calculate imposed electrostatic force for each individual participant by assuming ellipsoidal geometry (24) of the finger with semi-axes lengths as reported in Table 1 and §2.2. See Fig. 5 for comparison with experimental measurements.

3.2.4. Assessment of numerical implementation

Numerical models implemented in the finite element analysis in terms of (9b) and (9a) were assessed both against the analytical predictions and experimental results. Different tactile scenarios were considered, namely (i) tribometer experiments and voltage dependence of the imposed electrostatic force as reported in [13]; and (ii) hovering finger as in current experimental setup.

In-contact state. The computational framework output was verified against experimental results reported by Meyer et al. [13] in a similar manner as analytical models (§3.2.2). The framework was employed using the input parameters as reported ($d^{\mathrm{i}} = 1$ μm, $d^{\mathrm{sc}} = 200$ μm and $f = 10$ kHz) and

obtained results were compared with reported electrostatic forces (Fig. 7). Forces in 2D model are given in N/mm, therefore cannot be directly compared with the experimental results without assuming the appropriate contributing out-of-plane width, for which ≈ 10 mm represents a realistic approximation.

Out-of-contact state. Analogous scenarios as in experimental procedure were considered in numerical simulations: (i) the applied voltage U was kept constant at 2000 V and the finger was moved from 1.00 mm towards the plate until the contact was detected; (ii) the finger pad distance d^{a} was kept constant at 0.25 mm and the applied voltage was varied from 0 to 2500 V. The numerically obtained values were compared to experimental measurements and analytical predictions assuming ellipsoidal geometry of the finger (§3.2.3) at HVHD, HVLD and LVLD positions (Fig. 5 – *green* boxes), with out-of-plane width varying from $8 - 10$ mm.

3.2.5. Influence of the air layer d^{a} in in-contact state

The influence of the air layer on imposed electrostatic force for in-contact state was assessed numerically by performing a series of simulations using a developed finite element framework.

Simulation procedure is the following: the finger pad is pressed against the plate with desired normal force (0.1 to 1.0 N in a step of 0.1 N), before the effective voltage of 1000 V is applied. The imposed electrostatic force was determined for four cases: finger pad with and without fingerprints and with and without air layer, i.e. the electrostatic force was evaluated using either (9b) or (10).

The relative contribution of air layer to the total electrostatic force, i.e. the nominal difference between ${}^{h}\bar{F}_e^{\mathrm{K}}$ and ${}^{h}F_e^{\mathrm{K}}$, for the cases with and without finger prints is depicted in Fig. 11a, together with the fit to the proposed expression (11).

The study shows that considering the electrostatic force at nodes which are not in direct contact with the surface contributes significantly to the total electrostatic force (Fig. 11a). Their contribution to ${}^{h}\bar{F}_e$ levels at around 15 % and 40 % in case without and with finger prints, respectively, (Fig. 11b), hence, increase in the frictional force at vertical force values typically used for light touch exploration, (~ 0.5 N, i.e. 0.05 N/mm), is of the order of $10 - 20$ %.

3.3. Haptic rendering

Here, two examples of using the developed simulation framework as a virtual prototyping tool for texture encoding are presented (§2.3.4): simulation of sliding over a flat surface featuring a sharp transition in friction coefficients (§3.3.1) and simulation of sliding over a texture with distinct geometrical asperities (§3.3.2).

The procedure is the following: first, the analysis is performed using a reference standard, i.e. the surface is modelled as it appears in its physical form. The finger is indented until the prescribed

vertical displacement is reached, before it starts sliding horizontally across the surface. During the simulation, displacements, normal and friction force are monitored in constrained nodes of the finger pad (reference values). Next, the voltage profile, i.e. function of voltage in terms of central position of the finger pad, is calculated from referential friction force values using (20a).

The analysis procedure is then repeated: finger is indented towards the haptic display until the referential normal load is reached. During the sliding procedure, each incremental step is followed by application of the momentary electrostatic force force calculated from the voltage profile as a function of current position.

3.3.1. Surface transition

A reference standard with sharp transition in friction coefficients is considered, namely it increases from 0.5 to 0.6 at $x = 5$ mm. Fig. 12a depicts voltage profile, referential friction values and friction modulation induced by applied voltage.

Assuming haptic display has the same friction coefficient as reference standard at $x < 5$ mm, i.e. $\mu = 0.5$, the applied voltage at the moment of indentation is 0 V. Following the transition, the voltage is gradually increasing until it reaches the value of 1776.73 V, as calculated from (20a).[5] Pearson's correlation coefficient between referential and modulated friction equals 0.9995.

3.3.2. Sinusoidal texture

Here, we consider a reference standard with geometrical asperities that mimic real texture surface, parametrically described by

$$y(x) = 0.025(\sin 6x + \cos 12x - 1). \tag{25}$$

Supposing the friction coefficient of the haptic display equals or is greater than the one of the reference standard, the technique does not render the full experience of the texture, as applying the voltage cannot result into friction reduction. However, assuming the friction coefficient of the haptic display equals or is smaller than the minimal apparent friction coefficient (i.e quotient between momentary referential vertical and horizontal load), the voltage profile can be obtained in full. In the presented case, the coefficient of friction between a reference standard and finger pad is assumed to be 0.1, whereas minimal apparent friction coefficient equals 0.072.

The voltage profile is presented in Fig. 12b on the left in *red*, with referential friction values and friction modulation induced by applied voltage on the right. The modulated friction clearly reflects the induced voltage profile and gives a good fit to the referential values, i.e. Pearson's correlation coefficient between referential and modulated friction equals 0.988.

[5]Normal forces up to range 0.2 N are assumed, hence $k' = 112.0$ mm^2/N

Deformed shape of the finger pad during FE simulation is shown in Fig. 13. The figures depict the von Mises stress profile for the cases of a finger pad sliding over the reference standard and haptic display with applied electrostatic force. Note, that the difference in stresses profiles is due to the fact the voltage applied is the same for the whole haptic display and therefore renders the sensation of a real texture only when the finger is in motion, but provides no impression of geometrical asperities when the finger is static.

4. Discussion

This work proposes a novel two dimensional multi-physics electro-mechanical computational framework for simulating tactile scenarios and haptic rendering in electrovibration displays. In this context the mechanical and electrical properties of the finger pad and skin tissue are considered and the influence of the air layer as dielectric is quantified.

A literature review of the electrovibrations has been performed, with a focus on the analytical models used to elucidate experimental data. Two different analytical model to estimate the imposed electrostatic force have been proposed in the past by equations (3) and (5) with their extension to consider the air layer given, respectively, by equations (6) and (7). Regardless of the rather lengthy theoretical dispute about the correct mathematical description of the electrostatic force imposed on the finger pad, none of the relevant references provide the thorough comparison between the experimental results and the proposed analytical models. Both models are based on the infinite capacitor assumption and have been implemented in the above-mentioned framework, and their outputs have been compared with experimental values independently gathered and reported in the literature and current study. Although the modern textbooks [41] and research in electrostatic chucks support (6), the performed assessment clearly shows that in the case of electrovibration tactile displays the model (7) gives better estimation of the range of forces measured experimentally, especially in the relevant sliding scenarii.

A great emphasis was placed on modelling finger pad asperities and the profile of the *stratum corneum* due to its impact on magnitude of the electrostatic force, as even when the bodies are brought into contact, the air gaps are still present, arising from the difference between gross and real contact area [25]. Under infinite plate capacitor model with parallel dielectrics, an air layer between the finger pad and the plate also acts as a dielectric and contributes to the total electrostatic force. Although the relative permittivity of the air is in range with relative permittivity of the insulator, but relatively small when compared to the relative permittivity of the *stratum corneum*, the numerical analysis of light touch exploration shows that neglecting the air influence may lead to significant difference (cca. 20 %).

Although the electrovibration technique has already been implemented in prototype devices, in order to meet expectations of tomorrow's mass-market a transition from simple fingertip simulation to advanced tactile rendering is required. The implementation of a high fidelity texture rendering system into tablets and mobile phones would result in a more intuitive interaction, enable more natural perception of virtual reality and rebalance the cognitive load, which is currently almost entirely held by the sense of vision.

A simplified linearised relationship for a required voltage U in order to reproduce a desired lateral force profile, given by expression (20a), has been derived. The principle could be implemented into a device equipped only with a finger position sensor and could render real textures based on the approach proposed by Robles-De-La-Torre and Hayward [1]. If a normal force sensor is also present in the device the linearised approximation is not required and equation (19) can be employed instead.

The proposed framework may find application in designing rich haptic stimuli in electrovibration devices in which the characterisation of mechanical and geometrical properties of the exploring finger and skin tissue is essential. The web tool for virtual rendering of the textures, which follows the approach described in §2.3, is already in development and available on-line [56]. In future work a library of textures will be generated and development and evaluation of such a haptic device is foreseen.

Acknowledgement

This work was supported by the European commission within the FP7-PEOPLE-317100 Prototouch project.

References

[1] G. Robles-De-La-Torre and V. Hayward. Force can overcome object geometry in the perception of shape through active touch. *Nature*, 412(6845):445–448, 2001. doi: 10.1038/35086588.

[2] M. Wiertlewski and V. Hayward. Mechanical behavior of the fingertip in the range of frequencies and displacements relevant to touch. *J Biomech*, 45(11):1869–1874, 2012. doi: 10.1016/j.jbiomech.2012.05.045.

[3] M. Wiertlewski, J. Lozada, and V. Hayward. The spatial spectrum of tangential skin displacement can encode tactual texture. *IEEE T Robot*, 27(3):461–472, 2011. doi: 10.1109/TRO.2011.2132830.

[4] M. Biet, F. Giraud, and B. Lemaire-Semail. Squeeze film effect for the design of an ultrasonic tactile plate. *IEEE T Ultrason Ferr*, 54(12):2678–2688, 2007. doi: 10.1109/TUFFC.2007.596.

[5] T. Sednaoui, E. Vezzoli, B. Dzidek, B. Lemaire-Semail, C. Chappaz, and M. Adams. Experimental evaluation of friction reduction in ultrasonic devices. In *WHC, 2015 IEEE*, pages 37–42, 2015. doi: 10.1109/WHC.2015.7177688.

[6] L. Winfield, J. Glassmire, J. Colgate, and M. Peshkin. T-PaD: Tactile pattern display through variable friction reduction. In *EuroHaptics Conference, 2007 and Symposium on Haptic Interfaces for Virtual Environment and Teleoperator Systems. World Haptics 2007. Second Joint*, pages 421–426. IEEE, 2007. doi: 10.1109/WHC.2007.105.

[7] A. K. Agarwal, K. Nammi, K. A. Kaczmarek, M. E. Tyler, and D. J. Beebe. A hybrid natural/artificial electrostatic actuator for tactile stimulation. In *Microtechnologies in Medicine & Biology 2nd Annual International IEEE-EMB Special Topic Conference on*, pages 341–345. IEEE, 2002. doi: 10.1109/MMB.2002.1002343.

[8] O. Bau, I. Poupyrev, A. Israr, and C. Harrison. Teslatouch: Electrovibration for touch surfaces. In *Proceedings of the 23rd Annual ACM Symposium on User Interface Software and Technology*, pages 283–292, 2010. doi: 10.1145/1866029.1866074.

[9] D. J. Beebe, L. A. Ruston, K. A. Kaczmarek, and M. E. Tyler. A polyimide-on-silicon electrostatic fingertip tactile display. In *Engineering in Medicine and Biology Society, 1995., IEEE 17th Annual Conference*, volume 2, pages 1545–1546. IEEE, 1995. doi: 10.1109/IEMBS.1995.579819.

[10] K. Kaczmarek, K. Nammi, A. Agarwal, M. Tyler, S. Haase, and D. Beebe. Polarity effect in electrovibration for tactile display. *IEEE T Bio-Med Eng*, 53(10):2047–2054, 2006. doi: 10.1109/TBME.2006.881804.

[11] S.-C. Kim, A. Israr, and I. Poupyrev. Tactile rendering of 3D features on touch surfaces. In *Proceedings of the 26th Annual ACM Symposium on User Interface Software and Technology*, pages 531–538, 2013. ISBN 978-1-4503-2268-3. doi: 10.1145/2501988.2502020.

[12] H. Kim, J. Kang, K. D. Kim, K. M. Lim, and J. Ryu. Method for providing electrovibration with uniform intensity. *IEEE T Haptics*, 8(4):492–6, 2015. doi: 10.1109/TOH.2015.2476810.

[13] D. J. Meyer, M. A. Peshkin, and J. E. Colgate. Fingertip friction modulation due to electrostatic attraction. In *WHC, 2013*, pages 43–48, 2013. doi: 10.1109/WHC.2013.6548382.

[14] Z. Radivojevic, P. Beecher, C. Bower, S. Haque, P. Andrew, T. Hasan, F. Bonaccorso, A. C. Ferrari, and B. Henson. Electrotactile touch surface by using transparent graphene. In *Proceedings of the 2012 Virtual Reality International Conference*, VRIC '12. ACM, 2012. doi: 10.1145/2331714.2331733.

[15] Z. Radivojevic, P. Beecher, C. Bower, D. Cotton, S. Haque, P. Andrew, B. Henson, S. A. Wall, I. S. Howard, J. N. Ingram, D. M. Wolpert, A. O. Salo, and T. Xue. 31.1: Invited paper: Programmable electrostatic surface for tactile perceptions. *SID Symposium Digest of Technical Papers*, 43(1):407–410, 2012. doi: 10.1002/j.2168-0159.2012.tb05802.x.

[16] R. M. Strong and D. Troxel. An electrotactile display. *IEEE T Man Machine*, 11(1):72–79, 1970. doi: 10.1109/TMMS.1970.299965.

[17] E. Vezzoli, M. Amberg, F. Giraud, and B. Lemaire-Semail. *Electrovibration Modeling Analysis*, volume 8619 of *Lecture Notes in Computer Science*, pages 369–376. Springer Berlin Heidelberg, 2014. doi: 10.1007/978-3-662-44196-$1_4$5.

[18] E. Vezzoli, W. Messaoud, M. Amberg, F. Giraud, B. Lemaire-Semail, and M. Bueno. Physical and perceptual independence of ultrasonic vibration and electrovibration for friction modulation. *IEEE T Haptics*, 8(2):235–239, 2015. doi: 10.1109/TOH.2015.2430353.

[19] A. Johnsen and K. Rahbek. A physical phenomenon and its applications to telegraphy, telephony, etc. *Electrical Engineers, Journal of the Institution of*, 61(320):713–725, 1923. doi: 10.1049/jiee-1.1923.0092.

[20] E. Mallinckrodt, A. L. Hughes, and W. Sleator. Perception by the skin of electrically induced vibrations. *Science*, 118(3062):277–278, 1953. doi: 10.1126/science.118.3062.277.

[21] S. Grimnes. Electrovibration, cutaneous sensation of microampere current. *Acta Physiol Scand*, 118:19–25, 1983. doi: 10.1111/j.1748-1716.1983.tb07235.x.

[22] H. Tang and D. J. Beebe. A microfabricated electrostatic haptic display for persons with visual impairments. *IEEE T Rehabil Eng*, 6(3):241–248, 1998. doi: 10.1109/86.712216.

[23] J. M. Romano and K. J. Kuchenbecker. Creating realistic virtual textures from contact acceleration data. *IEEE T Haptics*, 5(2):109–119, 2012. doi: 10.1109/TOH.2011.38.

[24] T. André, V. Lévesque, P. Hayward, V. Lefèvre, and J.-L. Thonnard. Effect of skin hydration on the dynamics of fingertip gripping contact. *J R Soc Interface*, 8:1574–1583, 2011. doi: 10.1098/rsif.2011.0086.

[25] M. J. Adams, S. A. Johnson, P. Lefèvre, V. Lévesque, V. Hayward, T. André, and J.-L. Thonnard. Finger pad friction and its role in grip and touch. *J R Soc Interface*, 10(80), 2012. doi: 10.1098/rsif.2012.0467.

[26] D. J. Meyer. Electrostatic force on a human fingertip. Master's thesis, Northwestern University, 2012.

[27] C. D. Shultz, M. A. Peshkin, and J. E. Colgate. Surface haptics via electroadhesion: Expanding electrovibration with Johnsen and Rahbek. In *WHC, 2015 IEEE*, pages 57–62, 2015. doi: 10.1109/WHC.2015.7177691.

[28] K. Dandekar. *Role of mechanics in tactile sensing of shape*. PhD thesis, Massachusetts Institute of Technology, Department of Mechanical Engineering, 1995.

[29] K. Dandekar, B. I. Raju, and M. A. Srinivasan. 3-D finite-element models of human and monkey fingertips to investigate the mechanics of tactile sense. *J Biomech Eng-T Asme*, 125:682–691, 2003. doi: 10.1115/1.1613673.

[30] G. J. Gerling and G. W. Thomas. Fingerprint lines may not directly affect SA-I mechanoreceptor response. *Somatosens Mot Res*, 25(1):61–76, 2008. doi: 10.1080/08990220701838996.

[31] G. J. Gerling. SA-I mechanoreceptor position in fingertip skin may impact sensitivity to edge stimuli. *Appl Bionics Biomech*, 7(1):19–29, 2010. doi: 10.1080/11762320903069992.

[32] T. Maeno, K. Kobayashi, and N. Yamazaki. Relationship between the structure of human finger tissue and the location of tactile receptors. *JSME Int J C-Dyn Con*, 41(1):94–100, 1998. doi: 10.1299/kikaic.64.4798.

[33] D. D. Somer, D. Peric, E. de Souza Neto, and W. G. Dettmer. A multi-scale computational assessment of channel gating assumptions within the Meissner corpuscle. *J Biomech*, 48(1):73–80, 2015. doi: 10.1016/j.jbiomech.2014.11.003.

[34] T. Vodlak, Z. Vidrih, P. Pirih, A. Skorjanc, J. Presern, and T. Rodic. *Functional Microanatomical Model of Meissner Corpuscle*, volume 8619 of *Lecture Notes in Computer Science*, pages 377–384. Springer Berlin Heidelberg, 2014. doi: 10.1007/978-3-662-44196-$1_4$6.

[35] T. Vodlak, Z. Vidrih, D. Fetih, D. Peric, and T. Rodic. Development of a finite element model of a finger pad for biomechanics of human tactile sensations. In *EMBC, 2015 37th Annual International Conference of the IEEE*, pages 909–912, 2015. doi: 10.1109/EMBC.2015.7318510.

[36] M. B. Wagner, G. J. Gerling, and J. Scanlon. Validation of a 3-D finite element human fingerpad model composed of anatomically accurate tissue layers. In *Haptic interfaces for virtual environment and teleoperator systems, 2008. haptics 2008. symposium on*, pages 101–105, 2008. doi: 10.1109/HAPTICS.2008.4479922.

[37] J. Z. Wu, R. G. Dong, S. Rakheja, A. W. Schopper, and W. P. Smutz. A structural fingertip model for simulating of the biomechanics of tactile sensation. *Med Eng Phys*, 26(2):165–175, 2004. doi: 10.1016/j.medengphy.2003.09.004.

[38] J. Z. Wu, K. Krajnak, D. E. Welcome, and R. G. Dong. Analysis of the dynamic strains in a fingertip exposed to vibrations: Correlation to the mechanical stimuli on mechanoreceptors. *J Biomech*, 39(13):2445–2456, 2006. doi: 10.1016/j.jbiomech.2005.07.027.

[39] M. Abdolvahab. Rendering edge enhancement tactile phenomenon by friction variation in dynamic touch. *J Biomech*, 44(1):92–96, 2011. doi: 10.1016/j.jbiomech.2010.08.030.

[40] F. Giraud, M. Amberg, and B. Lemaire-Semail. Merging two tactile stimulation principles: electrovibration and squeeze film effect. In *WHC, 2013*, pages 199–203, 2013. doi: 10.1109/WHC.2013.6548408.

[41] R. P. Feynman, R. B. Leighton, and M. Sands. *The Feynman Lectures on Physics*. Reading, Massachusetts: Addison-Wesley, 1963.

[42] G. Brandstetter and S. Govindjee. Chucking pressures for idealized Coulomb-type electrostatic chucks. Technical report, University of California, Berkeley. Structural Engineering Mechanics and Materials, 2011.

[43] MATLAB. *version 8.2 (R2013b)*. The MathWorks Inc., Natick, Massachusetts, 2013.

[44] I. Wolfram Research. *Mathematica*. Wolfram Research, Inc., Champaign, Illinois, version 11.0 edition, 2016.

[45] J. Korelc. *AceFEM System*. Wolfram Research, Inc., Champaign, Illinois, 3.3 edition, 2012.

[46] S. Giavazzi, M. F. Ganatea, M. Trkov, and P. Šuštarič. Inverse determination of viscoelastic properties of human fingertip skin. *RMZ - Materials and geoenvironment*, 57(1):1–16, 2010.

[47] H. Fruhstorfer, U. Abel, C.-D. Garthe, and A. Knüttel. Thickness of the stratum corneum of the volar fingertips. *Clin Anat*, 13(6):429–433, 2000. doi: 10.1002/1098-2353(2000)13:6¡429::AID-CA6¿3.0.CO;2-5.

[48] Y. Fung. *Biomechanics: Mechanical Properties of Living Tissues*. Springer New York, 1993. ISBN 9780387979472.

[49] R. Lapeer, P. Gasson, and V. Karri. Simulating plastic surgery: From human skin tensile tests, through hyperelastic finite element models to real-time haptics. *Prog Biophys Mol Bio*, 103(2–3): 208–216, 2010. doi: 10.1016/j.pbiomolbio.2010.09.013. Special Issue on Biomechanical Modelling of Soft Tissue Motion.

[50] E. A. de Souza Neto, D. Peric, M. Dutko, and D. R. J. Owen. Design of simple low order finite elements for large strain analysis of nearly incompressible solids. *Int J Solids Struct*, 33(20-22): 3277–3296, 1996. doi: 10.1016/0020-7683(95)00259-6.

[51] T. Doca, F. M. Andrade Pires, and J. M. A. Cesar de Sa. A frictional mortar contact approach for the analysis of large inelastic deformation problems. *Int J Solids Struct*, 51(9):1697–1715, 2014. doi: 10.1016/j.ijsolstr.2014.01.013.

[52] J. Lengiewicz, J. Korelc, and S. Stupkiewicz. Automation of finite element formulations for large deformation contact problems. *Int J Numer Meth Eng*, 85:1252–1279, 2011. doi: 10.1002/nme.3009.

[53] D. Miklavcic, N. Pavselj, and F. X. Hart. *Electric Properties of Tissues*. John Wiley & Sons, Inc., 2006. doi: 10.1002/9780471740360.ebs0403.

[54] U. H. Birgersson, E. Birgersson, and S. Ollmar. Estimating electrical properties and the thickness of skin with electrical impedance spectroscopy: Mathematical analysis and measurements. *Journal of Electrical Bioimpedance*, 3(1):51–60, 2012. doi: 10.5617/jeb.400.

[55] M. J. Adams. Understanding the generic influence of moisture on the friction of skin from the contact mechanics of the finger pad. London, United Kingdom, December 2014. IMechE: Recent Advances in the Tribology and Bioengineering of the Skin.

[56] Z. Vidrih and E. Vezzoli. *Electrovibration Signal Design A Simulative Approach*, volume 9775 of *Lecture Notes in Computer Science*, pages 304–314. Springer International Publishing, 2016. doi: 10.1007/978-3-319-42324-1$_3$0.

Table 1: Experimental measurements

	gender	age	dh	a_i [mm]	b_i [mm]	c_i [mm]	HVHD [mN]	LVLD [mN]	HVLD [mN]
i	m	33	right	19.18	13.09	26.19	2.50	1.55	4.00
ii	f	28	right	14.04	11.16	25.67	1.70	1.37	2.73
iii	m	26	right	17.65	12.41	24.25	1.98	1.67	3.41
iv	m	28	right	17.89	14.94	26.50	1.85	1.21	2.49
v	m	22	right	16.45	11.66	27.02	0.91	0.54	1.54
vi	f	23	right	16.25	11.40	25.26	1.47	0.75	2.02
vii	m	25	right	16.89	12.53	24.18	1.11	0.86	1.86
viii	m	32	right	16.78	13.20	28.52	2.57	1.45	3.92
ix	m	57	left	18.20	15.00	28.40	2.31	1.86	4.17
x	f	55	right	14.69	12.80	25.62	1.40	0.81	1.85
xi	m	26	right	15.46	12.49	24.99	2.06	2.42	4.42

dh - dominant hand (handedness)
a_i - lateral axis length of the finger cross-section at proximal nail fold
b_i - vertical axis length of finger cross-section at proximal nail fold
c_i - length of the finger between interphalangeal joint and the finger tip
HVHD - high voltage, high distance (2500 V, 0.50 mm)
LVLD - low voltage, low distance (1414 V, 0.25 mm)
HVLD - high voltage, low distance (2500 V, 0.25 mm)

Table 2: List of material, geometrical and electrical parameters and their values

	parameter name	value	
E^{sc}	Young's modulus of *stratum corneum*	1.000	MPa
E^{ed}	Young's modulus of epidermis	0.136	MPa
E^{d}	Young's modulus of dermis	0.080	MPa
E^{hd}	Young's modulus of hypodermis	0.034	MPa
E^{n}	Young's modulus of nail	17.000	MPa
ν^{sc}	Poisson's ratio of *stratum corneum*	0.30	
ν^{ed}	Poisson's ratio of epidermis	0.30	
ν^{d}	Poisson's ratio of dermis	0.48	
ν^{hd}	Poisson's ratio of hypodermis	0.48	
ν^{n}	Poisson's ratio of nail	0.30	
μ	coefficient of friction	0.30	
a	finger width	16.68	mm
b	finger height	12.79	mm
R_{w}	fingerprint ridge width	0.50	mm
R_{h}	fingerprint ridge height	0.15	mm
ϵ_0	vacuum permittivity	8.85E-12	F/m
ϵ^{sc}	relative permittivity of *stratum corneum*	1650.00	
ϵ^{i}	relative permittivity of insulator	3.35	
ϵ^{a}	relative permittivity of air	1.00	
d^{sc}	thickness of *stratum corneum*	0.38	mm
d^{i}	thickness of insulator	0.09	mm
d^{a}	thickness of air gap	0.25, 0.50	mm
U^{eff}	effective voltage	1414, 2000	V

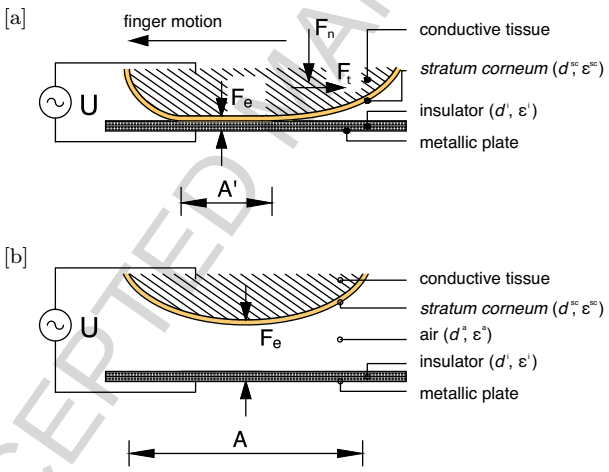

Figure 1: Schematic representation of standard capacitor system model for electrovibration in contact [a] and out-of-contact [b]. Note, that the nominal value of A is hard to estimate.

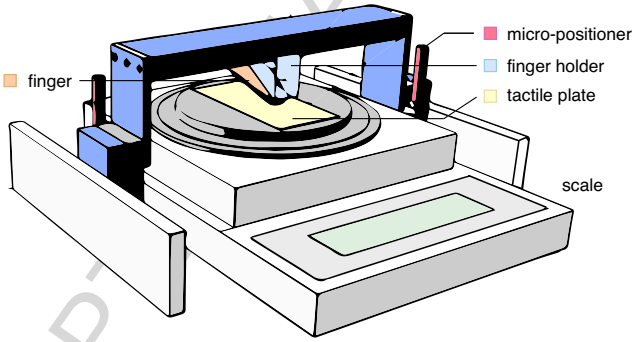

Figure 2: Experimental setup comprises a chemical scale acting as a force sensor and a bench installed over the scale. Finger-holder is attached to the bench with magnets. Vertical position of the finger is set by adjusting the micro-positioners installed on each side of the bench. Tactile plate placed on the scale and finger hovering above are not supposed to be brought in contact.

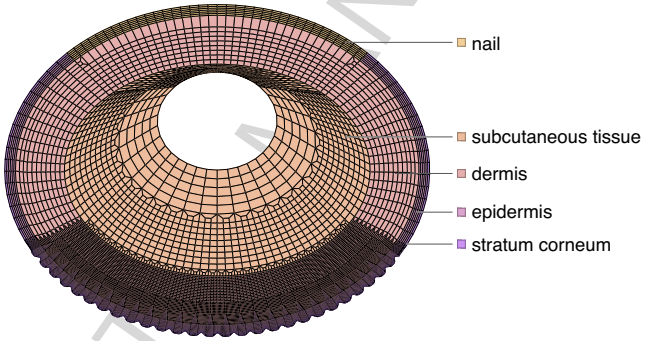

Figure 3: Schematic representation of the finger pad cross-section; the model comprises six characteristic domains: (i) stratum corneum, (ii) vital epidermis, (iii) dermis, (iv) hypodermis, (v) nail and (vi) bone. Figure depicts representative mesh of a 2D finite element model of a finger pad. The mechanical model of a finger pad employed in presented study is composed of 23,139 nodes and 21,150 elements. Stratum corneum consists of 2,240 nodes and 1,662 elements, epidermis of 10,998 nodes and 10,281 nodes, dermis of 8,208 nodes and 7,677 elements, hypodermis of 1,434 nodes and 1,314 elements, and nail consist of 259 nodes and 216 elements; bone is assumed to be rigid, therefore only fixed boundary conditions are prescribed at its contour.

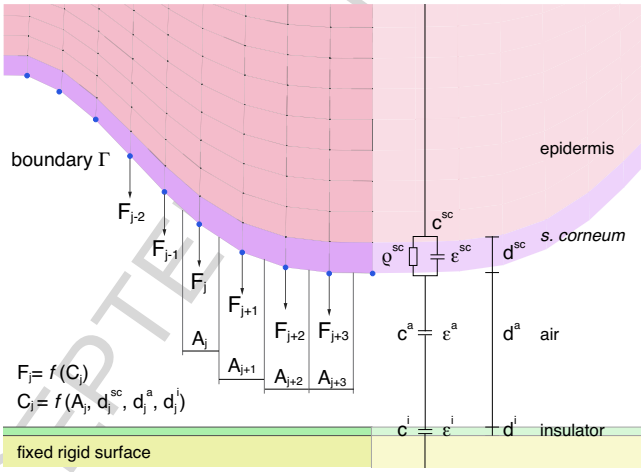

Figure 4: Schematic representation of implementation of the electrostatic component, based on the parallel plate capacitor assumption, within the finite contact element at the boundary Γ. For simplification the force is assumed to act on boundary nodes, i.e. nodes forming the potential contact between the finger pad and the surface.

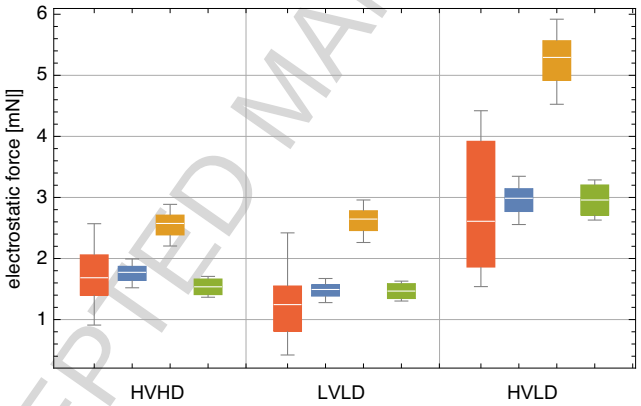

Figure 5: Box-whiskers chart around median confidence interval of electrostatic force for considered hovering scenarii: HVHD (2000 V, 0.50 mm), LVLD (1414 V, 0.25 mm) and HVLD (2000 V, 0.25 mm): experimental meassurements – *red*; analytical predictions calculated from (8b) – *blue* and (8a) – *orange* assuming elliptical model for each participant; numerical simulations using (7) – *green*.

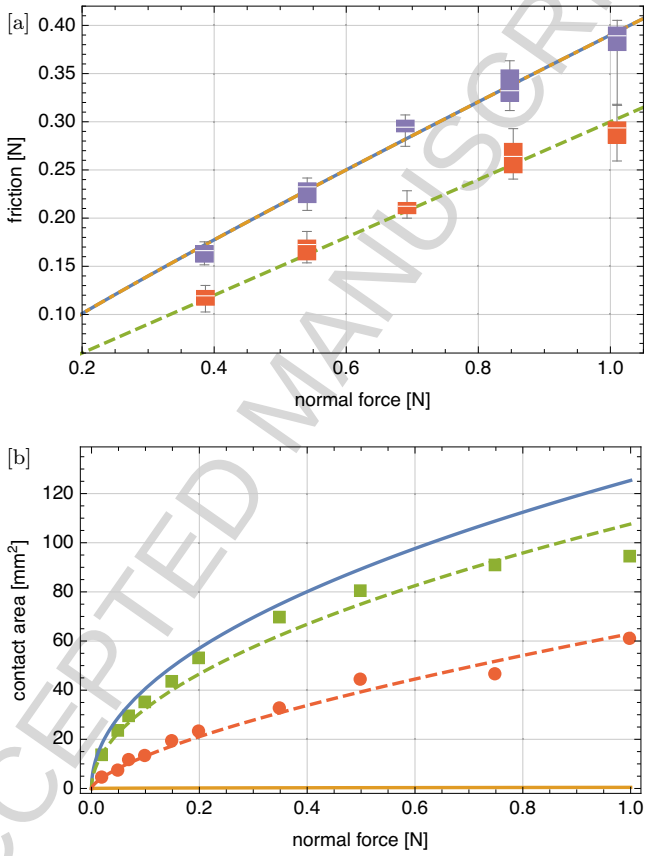

Figure 6: [a] Friction F_t as a function of normal force F_n: figure depicts box-whiskers chart around median confidence interval of experimental measurements [13] for the case of electrostatic on – *purple* and electrostatic off – *red* together with analytical fit $F_t = 0.3F_n$ – *green*; approximation to experimental measurements with electrostatic on is done by assuming power law for contact area, $A = kF_n^m$: $k = 0.446$ and $m = 0.489$ for (16b) – *orange*, and $k = 125.359$ and $m = 0.489$ for (16a) – *blue*. [b] Contact area as a function of normal force F_n obtained by fitting to experimental results: fit to (16b) – *orange* and fit to (16a) as above; measurements of gross – *green* and ridge – *red* contact area as reported in [55] together with power law approximation, $k = 107.626$, $m = 0.52$ and $k = 63.000$, $m = 0.68$, respectively.

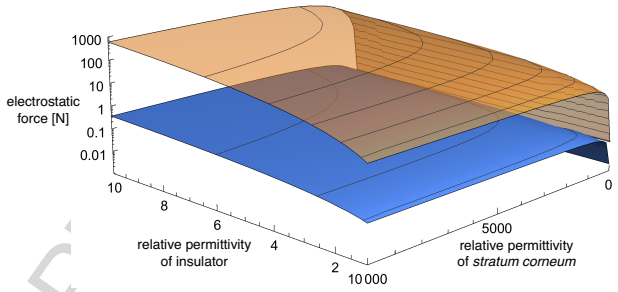

Figure 7: Imposed electrostatic force F_e as a function of ϵ^{sc} and ϵ^{i} for a typical range calculated from (3) – *orange*, and (5) – *blue*. Contact area A is assumed 100 mm^2, thicknesses of *stratum corneum* and insulator are 0.200 and 0.001 mm, respectively, and and effective voltage U_{eff} is 140 V. Note the logarithmic scale.

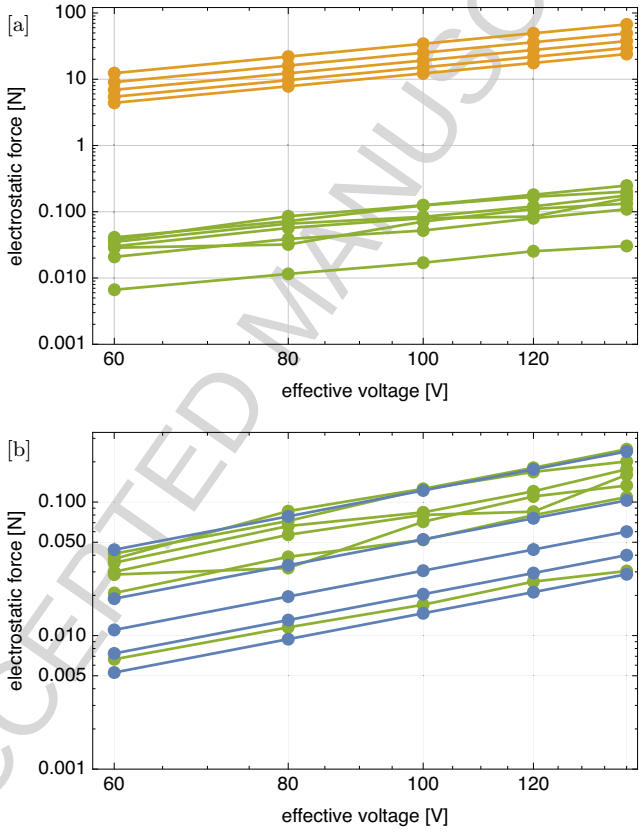

Figure 8: Imposed electrostatic force F_e as a function of applied voltage U calculated [a] using (3) – *orange*, and [b] using (5) – *blue*, for varying thickness of *stratum corneum* (from 0.1 to 0.5 in steps of 0.1 mm) and juxtaposed with experimental measurements reported by Meyer et al. [13] – *green*. Contact area A is assumed 100 mm^2, all other parameters as in Table 2. Note the logarithmic scale.

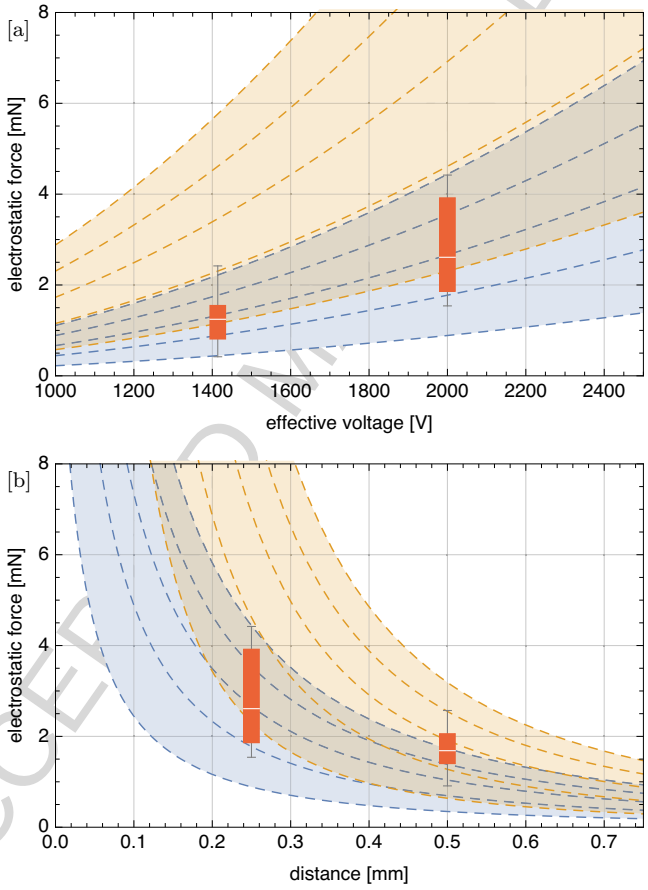

Figure 9: Comparison between experimental measurements – *red* and analytical predictions of electrostatic force F_e calculated using (3) – *orange*, and (5) – *blue*, as a function of [a] effective voltage, and [b] distance between the plate and the finger pad, under assumption of flat *stratum corneum* for different contributing areas A. As discussed earlier (Fig. 5), the *red* boxes show measurements for different loading scenarii: [a] HVLD and LVLD at 1414 and 2000 V, respectively, and [b] HVLD and HVHD at 0.25 and 0.50 mm, respectively.

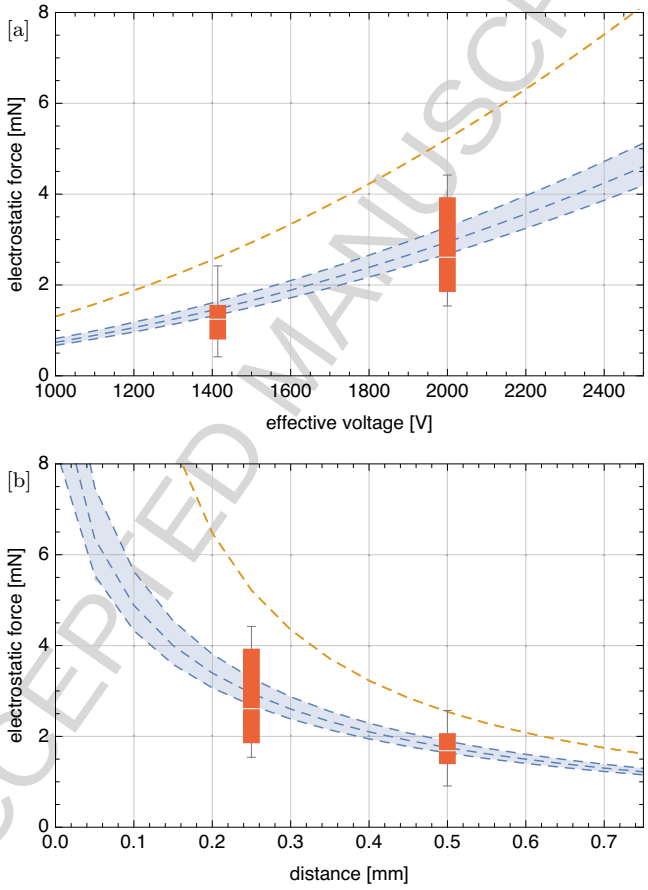

Figure 10: Comparison between experimental measurements – *red* and analytical predictions of electrostatic force F_e calculated using (3) – *orange*, and (5) – *blue*, as a function of [a] effective voltage, and [b] distance between the plate and the finger pad, under assumption of ellipsoidal geometry of the finger pad for different thicknesses of *stratum corneum*. As discussed earlier (Fig. 5), the *red* boxes show measurements for different loading scenarii: [a] HVLD and LVLD at 1414 and 2000 V, respectively, and [b] HVLD and HVHD at 0.25 and 0.50 mm, respectively.

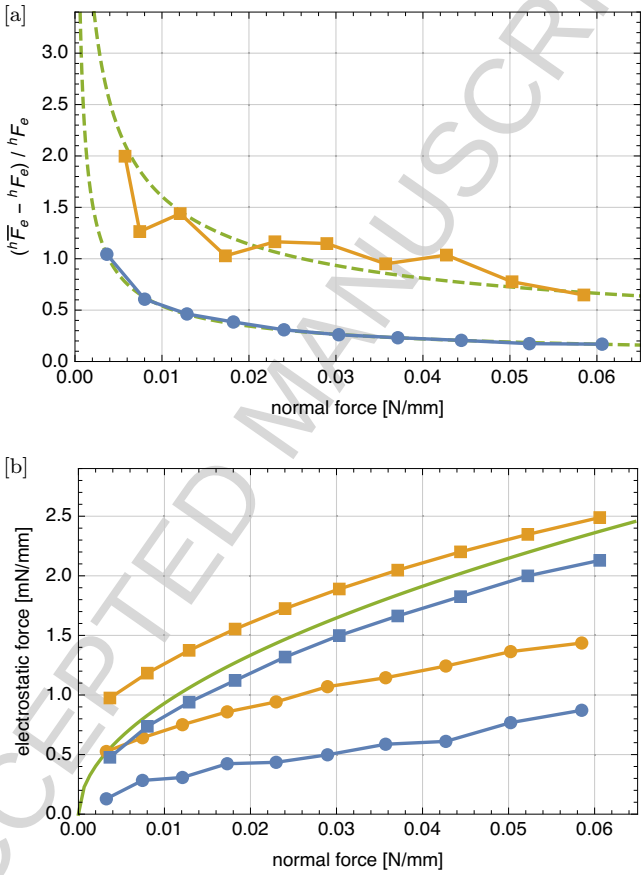

Figure 11: [a] Relative contribution of air layer to the electrostatic force in relation to normal force in case without fingerprint ridges – *blue* and with fingerprint ridges – *orange*. Fit to the proposed expression (11) – *green* gives parameter values $\alpha = 0.03$, $\beta = 0.65$ and $\alpha = 0.17$, $\beta = 0.49$ for the cases with and without fingerprint ridges, respectively. [b] Electrostatic force in relation to normal force for the cases when contribution of the air layer is considered $({}^{h}\bar{F}_e)$ – *orange* and when its influence is neglected $({}^{h}F_e)$ – *blue*. *Square* plot markers denote the simulation using the finger pad model without finger prints (i.e. $R_{\mathrm{h}} = 0$), while *circle* plot markers denote the simulation using the finger pad model with finger print ridges. *Green* solid line plots analytical prediction according to (7).

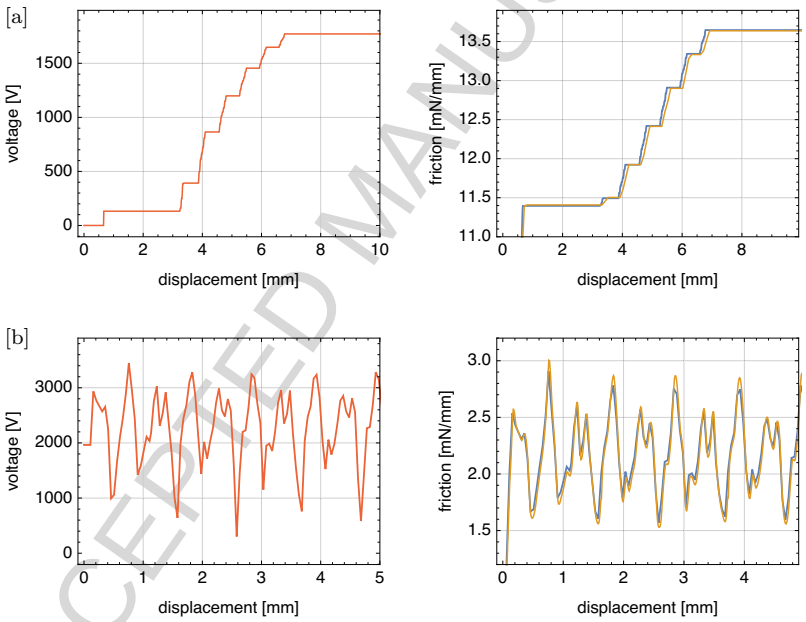

Figure 12: Haptic rendering of [a] flat surface with transition in friction from 0.5 to 0.6; [b] sinusoidal surface with sufficiently small coefficient of friction. Plots on the left in *red* show voltage scenario for each respective case calculated from (20a). Plots on right depicts frictional force as a function on finger position; reference values are plotted in *blue*, whereas modulated friction output is plotted in *orange*.

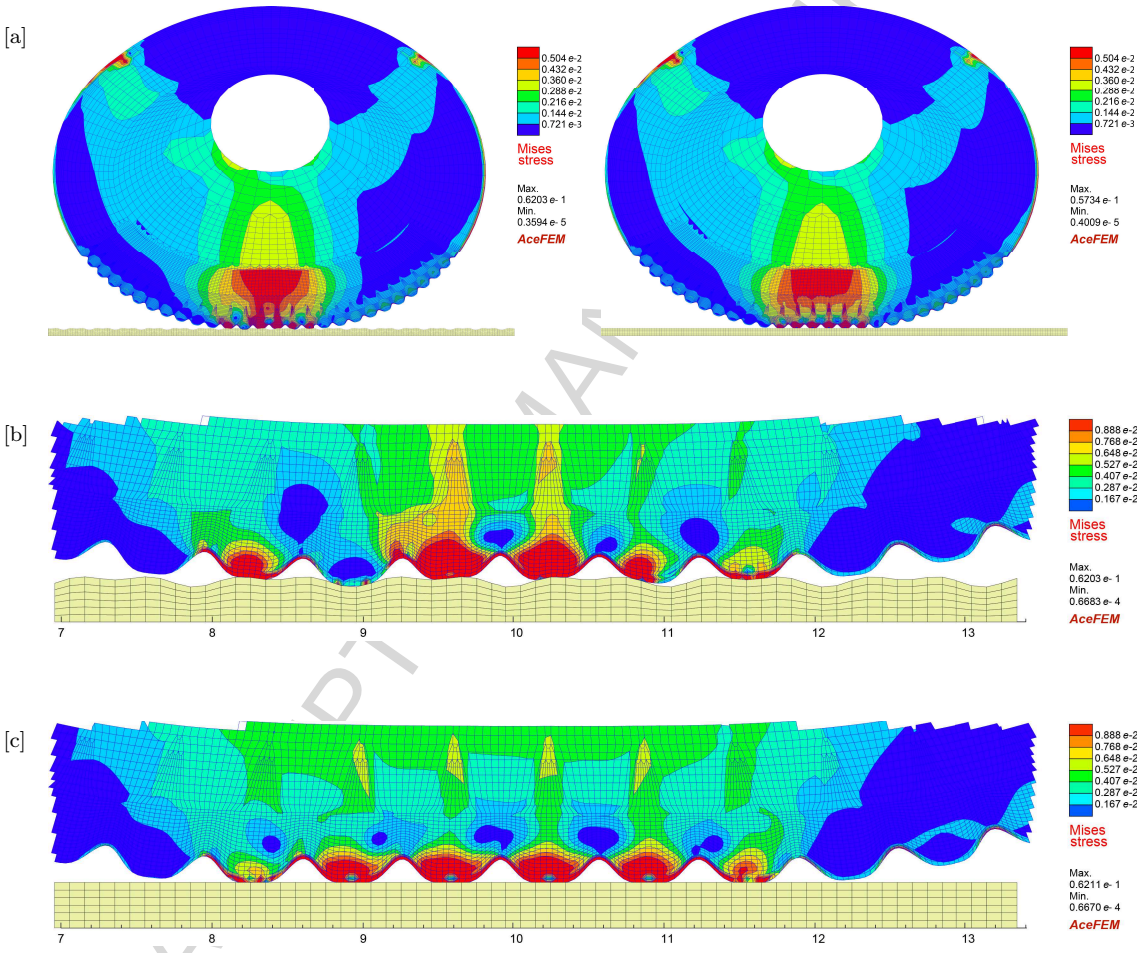

Figure 13: [a] Deformed shape of the finger pad sliding over the sinusoidal surface (left and closeup [b]) and corresponding situation of the finger pad sliding over the haptic display (right and closeup [c]). In case of haptic display, boundary nodes are additionally loaded with electrostatic force given in terms of applied voltage – the captured situation depicts application of 1911.12 V, calculated in terms of second voltage profile. i.e. coefficient of friction of the haptic display in this instant is $\mu \leq 0.072$. The contour plots in [a]-[c] represent the von Mises stresses.

.

Highlights

- experimental assessment of electrovibration analytical models is performed
- electrostatic force between finger pad and high voltage supplied plate was measured
- FE framework for tactile scenarios on real and virtual surfaces is presented
- an algorithm for haptic rendering using electrovibration technique is proposed
- influence of air-layer between finger pad and haptic display is investigated